

# Enhanced surface bombardment resistance of the CoNiCrFeMn high entropy alloy under extreme irradiation flux

Yangen Li<sup>1</sup>, Rui Li<sup>1,3</sup>  and Qing Peng<sup>2,3</sup> 

<sup>1</sup> School of Mechanical Engineering, University of Science and Technology Beijing, Beijing, 100083, People's Republic of China

<sup>2</sup> Nuclear Engineering and Radiological Sciences, University of Michigan, Ann Arbor, MI 48109, United States of America

E-mail: [lirui@ustb.edu.cn](mailto:lirui@ustb.edu.cn) and [qpeng@umich.edu](mailto:qpeng@umich.edu)

Received 5 June 2019, revised 17 August 2019

Accepted for publication 24 September 2019

Published 10 October 2019



## Abstract

We have investigated the response of the high entropy alloy of CoNiCrFeMn to the bombardment under extreme irradiation flux by means of molecular dynamics simulations. Compared to pristine Ni single crystalline, the CoNiCrFeMn HEA had less point defects during a single primary knock-on atom process. The average depth of defects was shallower. For consecutive bombardments, the CoNiCrFeMn HEA demonstrated much higher surface irradiation resistance than pristine Ni. Under the irradiation flux of  $5.59 \times 10^{27}$  n/(m<sup>2</sup>\*s), the number of defects in Ni gradually increased and was proportional to the number of bombardments, till the formation of dislocation which led to a boost of the defects. On the contrary, the number of defects in CoNiCrFeMn HEA was much less and stable, appearing to be insensitive to the number of bombardments and suggesting good radiation resistance. Such radiation resistance of CoNiCrFeMn HEA was attributed to the lattice distortion and sluggish diffusion of atoms, which could enhance the recombination of defects. Under the irradiation flux of  $1.68 \times 10^{28}$  n/(m<sup>2</sup>\*s), the boost of the defects in Ni occurred at lower number of bombardments. In addition, under both the irradiation flux of  $5.59 \times 10^{27}$  and  $1.68 \times 10^{28}$  n/(m<sup>2</sup>\*s), CoNiCrFeMn HEA had a smaller number of point defects and the defects were well dispersed. Our results showed that compared with Ni matrix, CoNiCrFeMn HEA had higher surface bombardment tolerance. This study might be helpful in the design of first-wall materials under the extreme irradiation flux.

Supplementary material for this article is available [online](#)

Keywords: irradiation, HEA, surface bombardment, point defects, extreme flux

(Some figures may appear in colour only in the online journal)

## 1. Introduction

It is a continuous and urgent desire to develop clean energy to support sustainable development of modern society. Among many candidates, nuclear energy is one of the most promising clean energies [1]. In the development of nuclear energy, one of the most essential issues is the first-wall materials. A

variety of energetic particles were produced in fusion reactors during operation. As a result, a large number of interstitial and vacancy defects occurred in the corresponding materials [2–4], then dislocation loops and surface defects would form [5]. Moreover, the next generation of fusion reactors was designed to have the high irradiation flux of  $10^{27} \sim 10^{29}$  n/(m<sup>2</sup>\*s) to increase efficiency, where the n referred to the number of incident particles [6–8]. In order to meet the challenges of high irradiation flux conditions, the

<sup>3</sup> Authors to whom any correspondence should be addressed.

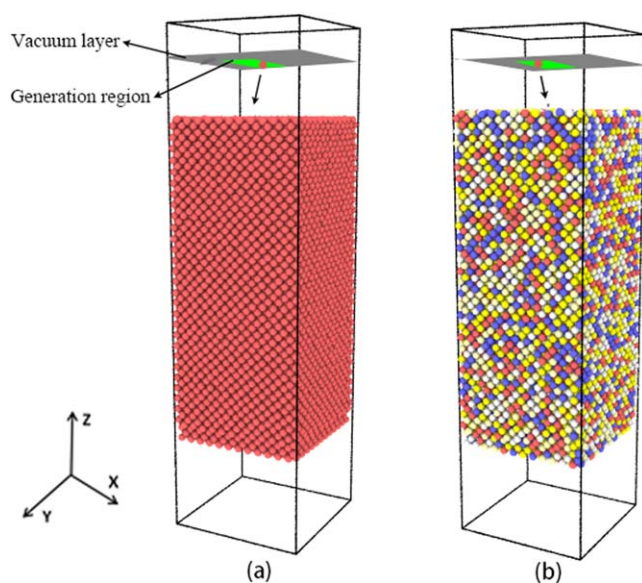


**Figure 1.** The models of Ni atom bombing the Matrix. The atom above the surface of the matrixes was Ni. (a) fcc-Ni; (b) fcc-CoNiCrFeMn HEA.

development of new irradiation tolerance first-wall materials was of great significance [9, 10].

High entropy alloy (HEA) was a new type of alloy that was the result of a combination of several various elements [11–13]. It has been showed that HEAs possessed excellent mechanical properties, good wear and corrosion as well as structural stability [14–17]. Moreover, HEA has proven to have high radiation damage tolerance [18, 19], and the factor for the well irradiation resistance was mainly due to the lattice distortion effects and sluggish diffusion effects [20–25]. As reported by Lu *et al* [26], the composition complexity and lattice distortion of HEA could reduce the migration and diffusion of defects, which provided effective trapping for the annihilation of freely migrating defects. Do *et al* [27] also indicated that the lattice distortion of HEA could result in a relatively limited collision space and a high recombination rate of defects. Therefore, HEA was a promising anti-irradiation first-wall material [28, 29].

Efforts have been made to study the anti-irradiation behavior of HEA [30–32]. However, the influences of the irradiation flux had not been systematically studied. Especially the irradiation resistance behavior of HEA under extreme condition of irradiation flux was seldom considered. In this paper, the evolution of defects in Ni and CoNiCrFeMn HEA under selected different irradiation flux was studied to explore the irradiation resistance behavior of HEA under energetic particles surface bombardment. The results showed that irradiation flux had a great influence on defects, and the CoNiCrFeMn HEA performed excellent than Ni matrix under extreme conditions.

## 2. Simulation models and method

Figures 1(a) and (b) showed the models of fcc-Ni and CoNiCrFeMn high entropy alloy, respectively. The number of Ni

atoms in model *a* was 17280. In model *b*, five types of atoms in the CoNiCrFeMn HEA were equally proportional and randomly distributed, with the total number of the atoms of 17 280. The dimensions of two models were the same, which were 4.23, 4.23, and 10.56 nm along *x*, *y*, and *z* directions, respectively. Periodic boundary conditions were applied along *x* and *y* directions. Ni atom was chosen as the incident atom because it was one component of both Ni and CoNiCrFeMn HEA. Two layers of atoms at the bottom of the sample box in two models were fixed to avoid the movement caused by the momentum from the incident Ni atoms. In order to prevent the atoms from bombarding the same surface position, the incident Ni atoms were generated with random direction and position in a 0.2 nm thick vacuum layer, which was 2 nm away from the top surfaces of matrixes, and then bombarded to the matrix. The incident energy of 3000 eV was applied because it was high enough to cause a large number of defects and would not penetrate the matrixes, and temperature of system 700 K was chosen to simulate the serious working situation [33].

2NN MEAM potential was applied to describe the interatomic interactions in the CoNiCrFeMn HEA as well as Ni matrix because it was proven to be suitable to simulation CoNiCrFeMn HEA [34]. In order to describe the short-range interatomic interaction in high-energy atomic collisions in cascades correctly, the *d* parameters in unary Co and Mn were adjusted from 0 to 0.03 and 0.02, respectively. Do *et al* [27] had confirmed that the change of *d* parameter was sufficient for short-range repulsion during atomic collisions, and it also had little effect on the fitted physical properties in each unary system. All the molecular dynamic simulations were conducted by LAMMPS [35]. The simulation systems were annealed with the NPT ensemble before conducting bombarding simulation. The time step was 0.001 ps. The annealing process was as follows. First, the simulation systems were relaxed at 300 K for 100 ps. Then the temperature of the systems was heated up to 2000 K at a rate of 3.4 K ps<sup>-1</sup>, and hold for 1000 ps to achieve equilibrium. Finally, the temperature was cooled down to 300 K at a rate of 3.4 K ps<sup>-1</sup>. The simulation of Ni irradiation was with the NVE ensemble, in which an adaptive time step was used so that each atom did not move more than 0.002 nm. The structure was relaxed for 2000 ps at temperature  $T = 700$  K to assure the system reach equilibrium before the bombarding process started. Berendsen thermostat was applied to the atoms with a thickness of 0.5 nm on each side of the matrix to avoid excessive thermal energy in the matrix during the irradiation process. The OVITO visualization tool [36] was used to analyze trajectories of the Ni atoms and the defects in the matrix.

## 3. Results and discussions

### 3.1. Irradiation resistance of two materials in a single bombardment

Surface bombardment simulations were carried out in two materials with an Ni atom with 3000 eV incident energy at

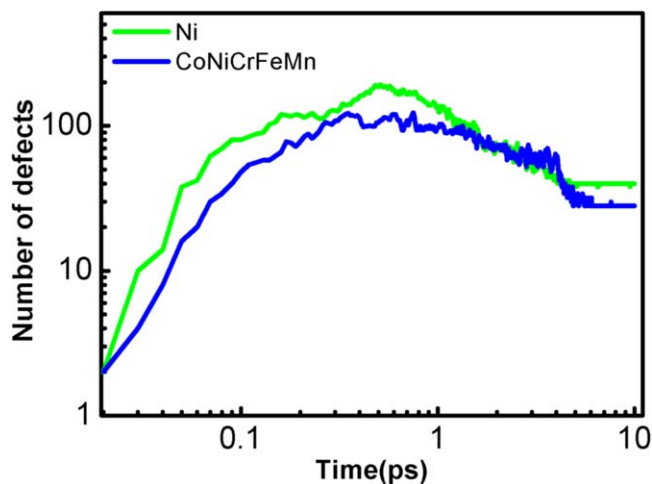


**Figure 2.** The number of defects of Ni and CoNiCrFeMn HEA during PKA process.

temperature  $T = 700$  K. During the primary knock-on atom (PKA) process, there were a series of events, such as cascade collision, the formation and relaxation of displacement spike, and the cooling of system to the ambient temperature. The point defects were produced and reached the peak due to the bombardment. Then the recombination of interstitials and vacancies occurred, and only a small part of point defects remained. To analyze point defects, the Wigner–Seitz [37] was applied to calculate the number of interstitials and vacancies. The relaxed Ni and CoNiCrFeMn matrix were taken as the reference structures for Wigner–Seitz analysis. Figure 2 showed the generation and evolution of defects in the two models during one typical PKA process, which lasted for about 10 ps. In the beginning of PKA, the number of defects in Ni and the CoNiCrFeMn HEA both increased rapidly due to the cascade collision, and reached a peak at around 0.3 ps. Then the kinetic energy and potential energy generated through cascade collision were randomly dissipated and converted into heat energy. The displacement collision, the movement and annihilation of defects all occurred at 0.3–3 ps. Furthermore, the number of defects gradually decreased, and the system cooled down to the ambient temperature. Finally, most of the defects caused by cascade collision were restored, and a small part of the defects remained inside the matrixes. The fraction for the defects that remained in the Ni matrix and CoNiCrFeMn HEA to the defects in peak were 24.8% and 18.6%, respectively. Multiple PKA simulations were carried out to obtain the statistics value of defects. More simulation results are presented in figure 1 of the supplementary data files (available online at [stacks.iop.org/NANO/31/025703/mmedia](https://stacks.iop.org/NANO/31/025703/mmedia)). The average interstitial and vacancy defects remained in the CoNiCrFeMn HEA were  $11 \pm 3$  and  $13 \pm 3$ , respectively. The unequal number of the interstitials and vacancies was attributed to the fast migration of interstitials to the surface. The interstitial and vacancy defects in Ni matrix were  $21 \pm 4$  and  $26 \pm 5$ , respectively, which were substantially larger than those in the HEA. Therefore, we might conclude that the CoNiCrFeMn HEA

had much higher irradiation resistance to the energetic particle bombardment than Ni matrix.

The distribution of kinetic energies of atoms in the Ni and CoNiCrFeMn matrixes and the number of defects with the depth were shown in figure 3. When the displacement spike formed at  $t = 0.3$  ps, the depth of cascade collision in Ni matrix almost reached the bottom, as shown as figure 3(a). The distribution of defects versus the depth at  $t = 0.3$  ps in Ni matrix was shown in the figure 3(d). Most defects remained in the lower part of the Ni matrix. However, in the CoNiCrFeMn HEA, as shown as figures 3(e)–(h). Because of the effect of sluggish diffusion, the cascade collision was suppressed, and the cascade collision occurred mainly in the middle part of the matrix.

### 3.2. The irradiation flux effect

In this part, Ni and the CoNiCrFeMn HEA were bombarded by continuous Ni atoms to evaluate the irradiation resistance of these two materials. As discussed in part 3.1, 0.3, 3 and 10 ps were the crucial time for the evolution of defects in PKA process. Therefore, when the matrix was bombarded by continuous Ni atoms, time interval 0.3, 3 and 10 ps were chosen, which corresponded to the irradiation flux of  $1.68 \times 10^{29}$  n/(m<sup>2</sup>\*s),  $1.68 \times 10^{28}$  n/(m<sup>2</sup>\*s), and  $5.59 \times 10^{27}$  n/(m<sup>2</sup>\*s), respectively. 300 bombardments were carried out.

When the irradiation flux was  $5.59 \times 10^{27}$  n/(m<sup>2</sup>\*s), the number of defects caused by incident Ni atoms was shown in figure 4(a). For the Ni matrix, defects gradually increased following the irradiation process and reached 631 defects in the end. Moreover, after 90 consecutive bombardments, a sharp increase appeared in the number of defects. The defects in CoNiCrFeMn HEA showed different trend. The number of defects increased slowly and remained relatively stable in the end. After 300 consecutive bombardments, the number of defects was only around 210. The results showed the CoNiCrFeMn HEA had stable and less defects under consecutive high irradiation flux than Ni matrix.

When the irradiation flux was enhanced to  $1.68 \times 10^{28}$  n/(m<sup>2</sup>\*s), the number of defects of Ni and CoNiCrFeMn during consecutive bombardments was shown in figure 4(b). Similar to the case when the irradiation flux was  $5.59 \times 10^{27}$  n/(m<sup>2</sup>\*s), a sharp increase of defects in Ni matrix appeared at about 70 bombardments, and then the defects gradually increased to more than 850. For the CoNiCrFeMn HEA, the number of defects increased slowly and eventually remained stable at around 224. The result indicated that CoNiCrFeMn HEA showed stable performance even under extreme irradiation flux.

The different behaviors of Ni matrix and the CoNiCrFeMn HEA under consecutive bombardments could be attributed to the ability of movement and accumulation of defects in materials. Consecutive bombardments of the Ni atoms caused more damage of Ni matrix than CoNiCrFeMn HEA, which contained five types of elements. The different atom sizes in the HEA caused large lattice distortion effect, leading to the less number of defects in the material after

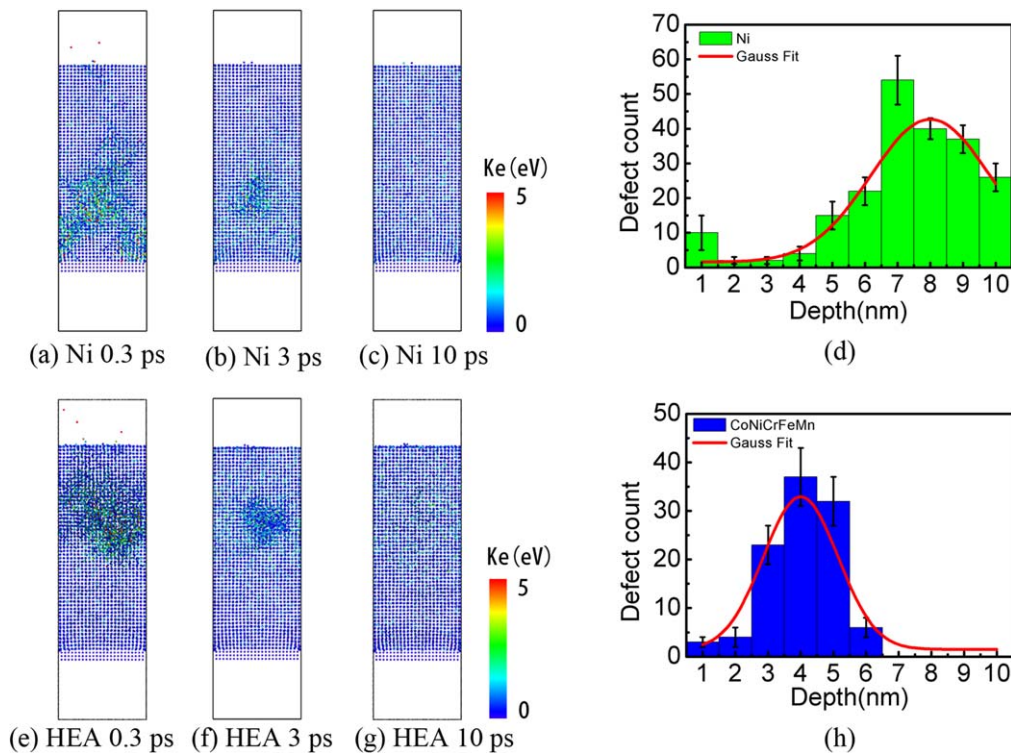


**Figure 3.** Kinetic energy distribution of the atoms in Ni (a) 0.3 ps; (b) 3 ps; (c) 10 ps; and CoNiCrFeMn HEA (e) 0.3 ps; (f) 3 ps; (g) 10 ps. The distribution of defects in (d) Ni and (h) CoNiCrFeMn HEA at  $t = 0.3$  ps, in which the displacement spike occurred.

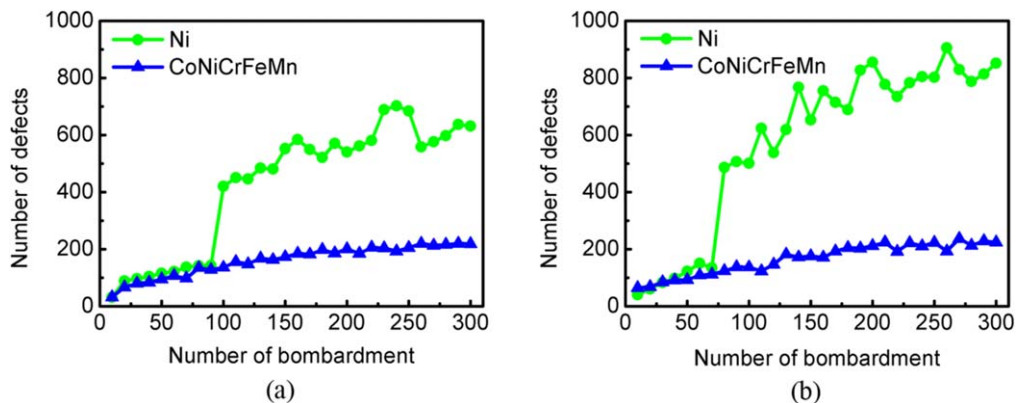


**Figure 4.** Defects of Ni and CoNiCrFeMn matrix during consecutive bombardments under the irradiation flux of (a)  $5.59 \times 10^{27} \text{ n}/(\text{m}^2 \cdot \text{s})$  and (b)  $1.68 \times 10^{28} \text{ n}/(\text{m}^2 \cdot \text{s})$ .

bombardment. At the same time, due to the sluggish diffusion effect of HEA, the effective diffusion rate between atoms was seriously affected, and the movement of defects was effectively suppressed. Therefore, defects in CoNiCrFeMn HEA increased slowly and remained relatively stable.

To find out why the sharp increase of defects in Ni matrix appeared during the bombardment process, we examined the dislocation loops when the sharp increase occurred under different irradiation flux, which were shown in figures 5(a) and (b). The formation of dislocation could be observed, and the dislocation slipped down to the deeper position during the bombardment. The formation and slip of the dislocations

produced a large number of surface defects and dislocation loops in Ni matrix, which led to the sharp increase of defects.

The distributions of the interstitials and vacancies in Ni matrix and CoNiCrFeMn HEA after 300 bombardments under the irradiation flux of  $5.59 \times 10^{27}$  and  $1.68 \times 10^{28} \text{ n}/(\text{m}^2 \cdot \text{s})$  were shown in figures 5(c) and (d). Under two kinds of irradiation flux, the distribution of defects in CoNiCrFeMn HEA was dispersed, which was considerably different with the defects in Ni matrix with concentrated distribution. Moreover, two obvious stacking fault interfaces could be observed inside Ni matrix.

When the irradiation flux increased to  $1.68 \times 10^{29} \text{ n}/(\text{m}^2 \cdot \text{s})$ , the second bombardment started after the

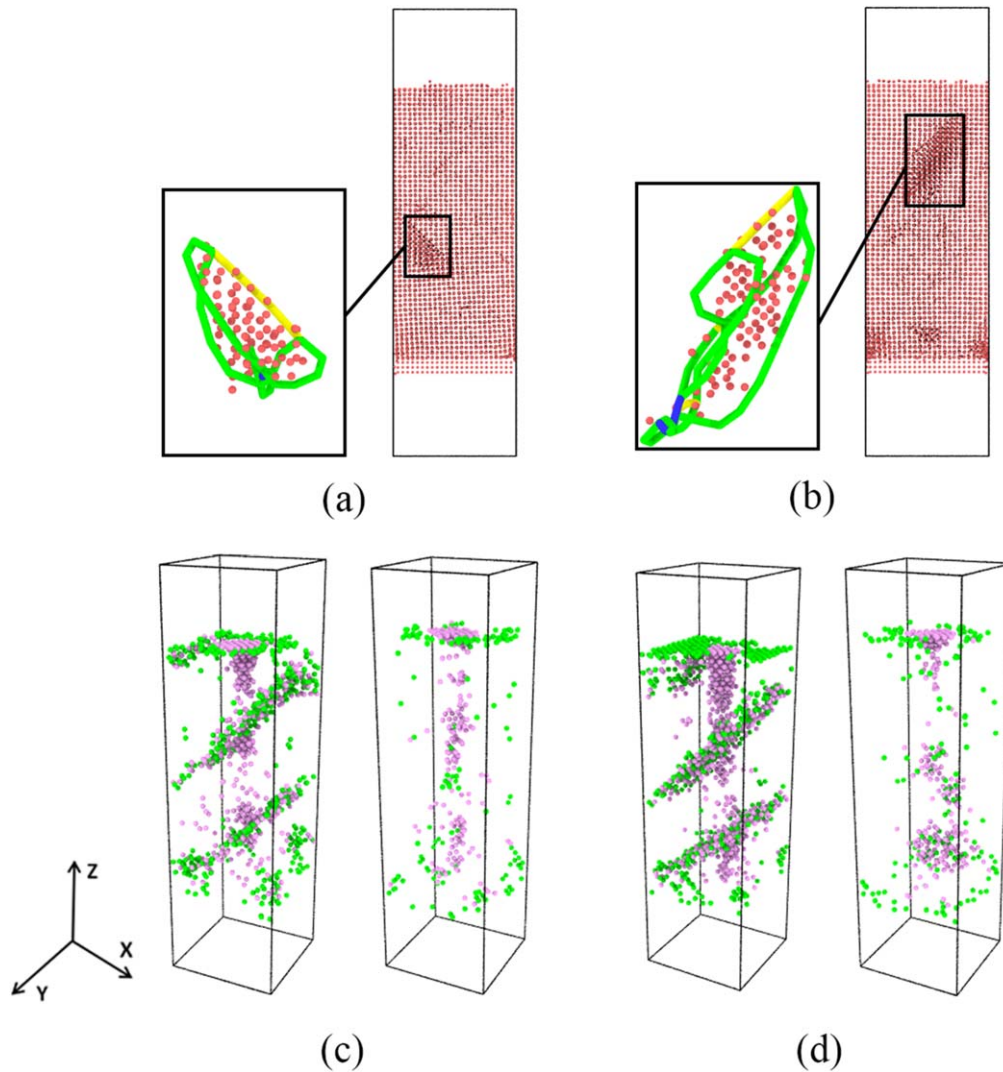


**Figure 5.** The dislocation loops in Ni matrix when the sharp increase of defects occurred. (a) After 90 bombardments under the irradiation flux of  $5.59 \times 10^{27} \text{ n}/(\text{m}^2 \cdot \text{s})$ . (b) After 70 bombardments under the irradiation flux of  $1.68 \times 10^{28} \text{ n}/(\text{m}^2 \cdot \text{s})$ . (The lines of different color represented different kinds of dislocation loops, where blue was Perfect, green was Shockley, yellow was Hirth); (c) and (d) showed the distribution of defects in Ni (left) and CoNiCrFeMn HEA (right) after 300 bombardments under different irradiation flux. (c) The irradiation flux was  $5.59 \times 10^{27} \text{ n}/(\text{m}^2 \cdot \text{s})$ ; (d)  $1.68 \times 10^{28} \text{ n}/(\text{m}^2 \cdot \text{s})$ . Pink and green balls denote vacancy and interstitial defects, respectively.

displacement spike just formed in initial PKA. Therefore, the systems did not have time to relax, and the cascade collision went on continuously. A big hole formed in the middle of Ni matrix and the matrix quickly swelled and was damaged after 5 bombardments, while the CoNiCrFeMn HEA could withstand 12 bombardments. The details of the result were provided in the figure 2 of the supplementary files.

#### 4. Conclusion



The surface bombardment process of fcc-Ni and CoNiCrFeMn HEA matrixes under extreme irradiation flux has been investigated by molecular dynamics simulations. We focused on the irradiation flux effect, which was modeled via consecutive bombardments with constant time separation. When the irradiation flux was  $5.59 \times 10^{27}$  and  $1.68 \times 10^{28}$

$\text{n}/(\text{m}^2 \cdot \text{s})$ , a sharp increase of the number of defects appeared in Ni matrix. The dislocation analysis revealed that such a boost of defects was due to the formation and slip of dislocations occurred in Ni matrix. However, the generation of point defects in HEA was relatively stable. The number of generated defects was considerably smaller than that in Ni matrix. Moreover, the defects in CoNiCrFeMn HEA were dispersed. On the contrary, two stacking fault interfaces were inside Ni matrix. When the irradiation flux was as high as  $1.68 \times 10^{29} \text{ n}/(\text{m}^2 \cdot \text{s})$ , the time interval was close to the formation of displacement spike in PKA. Ni matrix was damaged quickly after five bombardments, while CoNiCrFeMn HEA could withstand 12 bombardments. Our study illustrated that the CoNiCrFeMn HEA had much higher surface bombardment resistance than Ni matrix under the extreme irradiation flux, implying its potential applications as irradiation tolerant first-wall materials.

## Acknowledgments

The work is supported by the National Natural Science Foundation of China (No. 51475039).

## ORCID iDs

Rui Li  <https://orcid.org/0000-0003-0258-281X>  
 Qing Peng  <https://orcid.org/0000-0002-8281-8636>

## References

- [1] Budnitz R J 2016 Nuclear power: status report and future prospects *Energy Policy* **96** 735–9
- [2] Nordlund K, Ghaly M, Averback R, Caturla M, de La Rubia T D and Tarus J 1998 Defect production in collision cascades in elemental semiconductors and fcc metals *Phys. Rev. B* **57** 7556
- [3] Rong F C and Watkins G 1986 ODMR observation of close frenkel pairs in electron-irradiated ZnSe *Mater. Sci. Forum* **10** 827–32
- [4] Chant I and Murty K L 2010 Structural materials issues for the next generation fission reactors *JOM* **62** 67–74
- [5] Peng Q, Meng F, Yang Y, Lu C, Deng H, Wang L, De S and Gao F J 2018 Shockwave generates <100> dislocation loops in bcc iron *Nat. Commun.* **9** 4880
- [6] Zayachuk Y, Van Emmichoven P Z, Terentyev D, Uytendhouwen I and Van Oost G 2013 Surface modification of tungsten and tungsten–tantalum alloys exposed to high-flux deuterium plasma and its impact on deuterium retention *Nucl. Fusion* **53** 013013
- [7] Zayachuk Y, Manhard A, Jacob W, Van Emmichoven P Z and Van Oost G 2015 The effect of ion flux on plasma-induced modification and deuterium retention in tungsten and tungsten–tantalum alloys *J. Nucl. Mater.* **464** 69–72
- [8] Wu Y 2018 Development of high intensity D–T fusion neutro generator HINEG *Int. J. Energy Res.* **42** 68–72
- [9] Zinkle S J and Was G 2013 Materials challenges in nuclear energy *Acta Mater.* **61** 735–58
- [10] Zinkle S J and Snead L L 2014 Designing radiation resistance in materials for fusion energy *Annu. Rev. Mater. Res.* **44** 241–67
- [11] Miracle D B and Senkov O N 2017 A critical review of high entropy alloys and related concepts *Acta Mater.* **122** 448–511
- [12] Lu Y, Dong Y, Guo S, Jiang L, Kang H, Wang T, Wen B, Wang Z, Jie J and Cao Z 2014 A promising new class of high-temperature alloys: eutectic high-entropy alloys *Sci. Rep.* **4** 6200
- [13] Ye Y, Wang Q, Lu J, Liu C and Yang Y 2016 High-entropy alloy: challenges and prospects *Mater. Today* **19** 349–62
- [14] Tsai M-H 2013 Physical properties of high entropy alloys *Entropy* **15** 5338–45
- [15] Li Z, Pradeep K G, Deng Y, Raabe D and Tasan C C 2016 Metastable high-entropy dual-phase alloys overcome the strength–ductility trade-off *Nature* **534** 227–30
- [16] Wu Z, Bei H, Pharr G M and George E P 2014 Temperature dependence of the mechanical properties of equiatomic solid solution alloys with face-centered cubic crystal structures *Acta Mater.* **81** 428–41
- [17] Yeh J W, Chen S K, Lin S J, Gan J Y, Chin T S, Shun T T, Tsau C H and Chang S Y 2004 Nanostructured high-entropy alloys with multiple principal elements: novel alloy design concepts and outcomes *Adv. Energy Mater.* **6** 299–303
- [18] Wang X, Barr C M, Jin K, Bei H, Hattar K, Weber W J, Zhang Y and More K L 2019 Defect evolution in Ni and NiCoCr by *in situ* 2.8 MeV Au irradiation *J. Nucl. Mater.* **523** 502–9
- [19] Zhao S, Zhang Y and Weber W J 2018 Stability of vacancy-type defect clusters in Ni based on first-principles and molecular dynamics simulations *Scr. Mater.* **145** 71–5
- [20] Vaidya M, Trubel S, Murty B, Wilde G and Divinski S V 2016 Ni tracer diffusion in CoCrFeNi and CoCrFeMnNi high entropy alloys *J. Alloys Compd.* **688** 994–1001
- [21] Tsai K-Y, Tsai M-H and Yeh J-W 2013 Sluggish diffusion in Co–Cr–Fe–Mn–Ni high-entropy alloys *Acta Mater.* **61** 4887–97
- [22] Yeh J-W 2015 Physical metallurgy of high-entropy alloys *JOM* **67** 2254–61
- [23] Wang Z, Fang Q, Li J, Liu B and Liu Y 2018 Effect of lattice distortion on solid solution strengthening of BCC high-entropy alloys *J. Mater. Sci. Technol.* **34** 349–54
- [24] Lee C, Song G, Gao M C, Feng R, Chen P, Brechtel J, Chen Y, An K, Guo W and Poplawsky J D 2018 Lattice distortion in a strong and ductile refractory high-entropy alloy *Acta Mater.* **160** 158–72
- [25] Kucza W, Dąbrowa J, Cieślak G, Berent K, Kulik T and Danielewski M 2018 Studies of ‘sluggish diffusion’ effect in Co–Cr–Fe–Mn–Ni, Co–Cr–Fe–Ni and Co–Fe–Mn–Ni high entropy alloys; determination of tracer diffusivities by combinatorial approach *J. Alloys Compd.* **731** 920–8
- [26] Lu C, Niu L, Chen N, Jin K, Yang T, Xiu P, Zhang Y, Gao F, Bei H and Shi S 2016 Enhancing radiation tolerance by controlling defect mobility and migration pathways in multicomponent single-phase alloys *Nat. Commun.* **7** 13564
- [27] Do H-S and Lee B-J 2018 Origin of radiation resistance in multi-principal element alloys *Sci. Rep.* **8** 16015
- [28] He M-R, Wang S, Shi S, Jin K, Bei H, Yasuda K, Matsumura S, Higashida K and Robertson I M 2017 Mechanisms of radiation-induced segregation in CrFeCoNi-based single-phase concentrated solid solution alloys *Acta Mater.* **126** 182–93
- [29] Yang T, Xia S, Liu S, Wang C, Liu S, Fang Y, Zhang Y, Xue J, Yan S and Wang Y 2016 Precipitation behavior of Al<sub>x</sub>CoCrFeNi high entropy alloys under ion irradiation *Sci. Rep.* **6** 32146
- [30] Ullah M W, Xue H, Velisa G, Jin K, Bei H, Weber W J and Zhang Y 2017 Effects of chemical alternation on damage accumulation in concentrated solid-solution alloys *Sci. Rep.* **7** 4146
- [31] Levo E, Granberg F, Fridlund C, Nordlund K and Djurabekova F 2017 Radiation damage buildup and dislocation evolution in Ni and equiatomic multicomponent Ni-based alloys *J. Nucl. Mater.* **490** 323–32
- [32] Yang T, Xia S, Guo W, Hu R, Poplawsky J D, Sha G, Fang Y, Yan Z, Wang C and Li C 2018 Effects of temperature on the irradiation responses of Al<sub>0.1</sub>CoCrFeNi high entropy alloy *Scripta Mater.* **144** 31–5
- [33] Guérin Y, Was G S and Zinkle S J 2009 Materials challenges for advanced nuclear energy systems *MRS Bull.* **34** 10–9
- [34] Choi W-M, Jo Y H, Sohn S S, Lee S and Lee B-J 2018 Understanding the physical metallurgy of the CoCrFeMnNi high-entropy alloy: an atomistic simulation study *NPJ Comput. Mater.* **4** 1
- [35] Plimpton S 1995 Fast parallel algorithms for short-range molecular dynamics *J. Comput. Phys.* **117** 1–19
- [36] Stukowski A 2009 Visualization and analysis of atomistic simulation data with OVITO—the open visualization tool *Modelling Simul. Mater. Sci.* **18** 015012
- [37] Stefanou N, Akai H and Zeller R 1990 An efficient numerical method to calculate shape truncation functions for Wigner–Seitz atomic polyhedra *Comput. Phys. Commun.* **60** 231–8